2014

Quartz Hodoscope: Assembly, Calibration, And Data Analysis

Julian T. Wilson
North Carolina Agricultural and Technical State University

Quartz Hodoscope: Assembly, Calibration, and Data Analysis

Julian T. Wilson

North Carolina A&T State University

A thesis submitted to the graduate faculty

in partial fulfillment of the requirements for the degree of

MASTER OF SCIENCE

Department: Physics

Major: Physics

Major Professor: Dr. Abdellah Ahmidouch

Greensboro, North Carolina

2014

The Graduate School
North Carolina Agricultural and Technical State University

This is to certify that the Master's Thesis of

Julian T. Wilson

has met the thesis requirements of
North Carolina Agricultural and Technical State University

Greensboro, North Carolina
2014

Approved by:

Dr. Abdellah Ahmidouch Major Professor	Dr. Samuel Danagoulian Committee Member
Dr. Floyd James Committee Member	Dr. Abdellah Ahmidouch Department Chair
Dr. Sanjiv Sarin Dean, The Graduate School	

Biographical Sketch

Julian T. Wilson was born in Atlanta, GA on June 7, 1988. He attained his undergraduate degree at Morehouse College in Physics. He is a candidate for the Master of Science degree in Physics at North Carolina A&T State University.

Dedication

You have to be persistent to get anywhere in life. To all of those going through tough times, don’t give up.

Acknowledgments

I would like to thank my advisor, Dr. Abdellah Ahmidouch and co-advisor Dr. Samuel Danagoulian, for the guidance, encouragement and support while I was pursuing my thesis research at North Carolina Agricultural and Technical State University.

I'd like to say thank you to my parents, Harold & Cassandra Wilson. They've been behind me from day 1 in pushing me to pursue higher education and following my dreams. You guys have sacrificed so much to give me a chance to do something great, and I may never be able to thank you enough. Thanks to my sister Simone and her family for their support and prayers. To all my friends and extended family, you guys mean the world to me.

The major funding for this research has been secured from the National Science Foundation award # PHY 110123 to the Nuclear Physics Group (A. Ahmidouch and S. Danagoulian). The award sustained the group scientific research at Jefferson Laboratory (Newport News, VA).

Table of Contents

List of Tables

List of Figures

Abstract

The quartz hodoscope, which is a major component of the trigger system in the Super High Momentum Spectrometer at Jefferson Lab, has been constructed, tested, and analyzed at North Carolina A&T State University. The SHMS spectrometer will play a major role in the 12-GeV physics program at Hall-C of Jefferson Lab. The hodoscope detector is comprised of twenty-one quartz bars, each connected to a pair of photomultiplier tubes. The detector uses Cherenkov radiation to allow for the clean and precise detection of high-energy particles and the suppression of background noise. The scientific motivation, hodoscope construction, and relevant results will be presented.

CHAPTER 1

Introduction

Thomas Jefferson National Accelerator Facility (JLab) is a national laboratory funded by the U.S. Department of Energy. The lab's primary directive is to conduct basic research in the nuclear physics field. Experiments performed at Jefferson Lab probe the building blocks of matter[1]. The lab uses a unique particle accelerator that employs a continuous beam of light directed at three potential targets housed in three distinct halls.

The lab uses an Electron Beam within the Continuous Electron Beam Accelerator Facility or CEBAF. This beam was used in experiments that measure among other things the structure of nuclei, protons, and neutrons. In order to pursue further developments and possibilities in the field of nuclear physics, Jefferson Lab is doubling the energy of the electron beam from 6 GeV to 12 GeV as well as constructing a new experiment hall on the campus. The upgrade will push researchers to new research frontiers in studying subatomic particles and their interactive forces.

One of the major upgrades happening in Hall-C experimental hall at Jefferson Lab is the construction of the Super High Momentum Spectrometer or shortly SHMS. The SHMS is a particle spectrometer, which has the ability to distinctively detect a charge particle, its nature, measure its energy, arrival time, as well as angle and track. A key component of the SHMS Detector system is its triggering system consisting of a series of detector planes, three scintillator planes and a quartz hodoscope. The hodoscope should yield a particle detection efficiency of close to 100% while also suppressing the background noise and providing accurate particle tracking determination.

The quartz hodoscope is being developed as a collaboration of North Carolina A&T State University and Jefferson Lab. This document will detail the construction, calibration, and results of the data analysis.

CHAPTER 2

Physics Motivation

2.1 12 GeV Upgrade

Jefferson Lab is currently undergoing an energy upgrade of the CEBAF complex. Until the year 2011 the CEBAF facility could accelerate the electron beam at up to an energy of 6 $(GeV/c)^2$. The upgrade will allow for linear acceleration at up to 12 $(GeV/c)^2$ which opens the door for new higher energy experiments in nuclear physics.

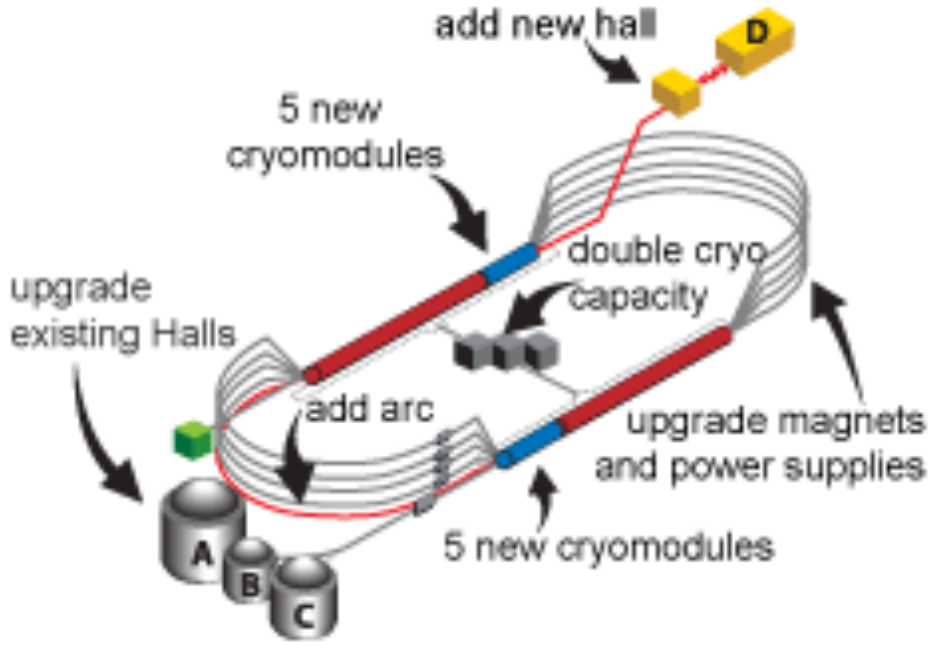

Figure 2.1. 12 GeV upgrade

This upgrade consists of adding 5 new cryomodules to each of the two linear accelerators, bringing the total up to twenty-five each. To manage the increased energy level, the cooling center is doubling its cryogenics capacity and the superconducting magnets on the recirculating

arcs are being upgraded as well. A new experimental Hall known as Hall D is being constructed to perform meson spectroscopy experiments in addition to upgrading the three current experimental halls, to complete the upgrade of the facility.

2.2 Upgrade Motivation

The 12 GeV upgrade to the Electron Beam at Jefferson Lab is an opportunity for scientists to perform unique and unprecedented experiments in the nuclear physics field. Researchers will be able to investigate the quark and gluon structure of strongly interacting systems and determine the validity of quantum chromodynamic theory or QCD. This theory, as well as describing strong particle interaction, should give a full description of quark systems. Specifically, the upgrade should provide evident developments in a few specific areas of nuclear physics[2].

- Researchers will be able to explore the intricate structure of QCD by searching for exotic mesons.
- Researchers will have the ability to explore beyond the standard of particle physics. By using the high precision studies of parity violation, researchers will have usage of an energy scale potentially even higher than that of the International Linear Collider.
- With unparalleled luminosity, duty factor, and kinematic reach far exceeding contemporarily available physics, the 12 GeV electron beam will grant researchers an unprecedented perspective into both the spin and flavor aspects of the valence parton distributions.
- Researchers will have a unique look into the atomic structure of nuclei, with the ability to explore how the valence quark structure is modified in a dense nuclear medium. This

research will soon give clearer and more significant understandings of the atomic structure of nuclei with potential implications for both nuclear physics and astrophysics.

- Researchers will have the ability to utilize nuclear tomography and discover the true three-dimensional structure of particles in the atomic nucleus.

2.3 Approved Experiments in Hall C

A series of experiments covering a wide range of physics topics have been approved to run in Hall-C. Table 2.1 provides a sample of these experiments.

Table 2.1

Partial list of approved experiments in Hall-C

Experiment	Title
E12-06-101[3]	Measurement of the Charged Pion Form Factor to High Q^2
E12-06-104[4]	Measurement of the Ratio $R = \sigma_L/\sigma_T$ in Semi-Inclusive Deep-Inelastic Scattering
E12-06-105[5]	Inclusive Scattering from Nuclei at $X > 1$ in the quasielastic and deeply inelastic regimes
E12-06-121[6]	A Path to "Color Polarizabilities" in the Neutron: A Precision Measurement of the Neutron g_2 and d_2 at High Q^2 in Hall C
E12-07-105[7]	Scaling Study of the L-T Separated Pion Electroproduction Cross Section at 11 GeV

2.4 Neutron Form Factor

One experiment in particular that will be focused on is the measurement of the Neutron Form Factor. This experiment will measure the Electric form factor for a neutron at a four-squared momentum transfer Q^2 of recoil polarimetry and a liquid deuterium target. Measuring the electric form factor of the neutron will give physicists a much deeper and clearer look at the fundamental elements behind nucleon and their nuclear structure. This new experiment proposes measurements of the G^n_E at up to 6.88, 5.22, 3.95 $(GeV/c)^2$.

This experiment will resolve the electric to magnetic form factor ratio from measurements of the neutron's recoil polarization in the quasielastic scattering of longitudinally polarized electrons from unpolarized neutrons in deuterium[3]. The transverse and longitudinal components of the neutron's recoil polarization are given by:

$$P_t = -2P_e G_E^n G_M^n K_t$$

$$P_\ell = 2P_e (G_M^n)^2 K_\ell$$

where P_e is the electron beam polarization, and K_t and K_l are electron kinematic factors[3].

Transmission through a vertical magnetic dipole field results in the recoil polarization vector precession through some angles χ, which lead to a scattering asymmetry $\xi(\chi)$ sensitive to the recoil polarizations P_t and P_l. The ratio of the G_E and G_m is then given by

$$g \equiv (\frac{G_E}{G_M}) = K_R \tan(\chi) \frac{(\eta + 1)}{(\eta - 1)}$$

with an asymmetry ratio of

$$\eta \equiv \frac{\xi_-}{\xi_+} = \frac{P_-^\chi}{P_+^\chi}$$

The experimental setup of the neutron form factor measurement uses a technique known as recoil polarimetry. This approach scatters polarized electrons off an unpolarized deuterium target. While the electrons will be detected by the SHMS spectrometer, the scattered neutrons will be detected by neutron polarimeter rendered below[3]:

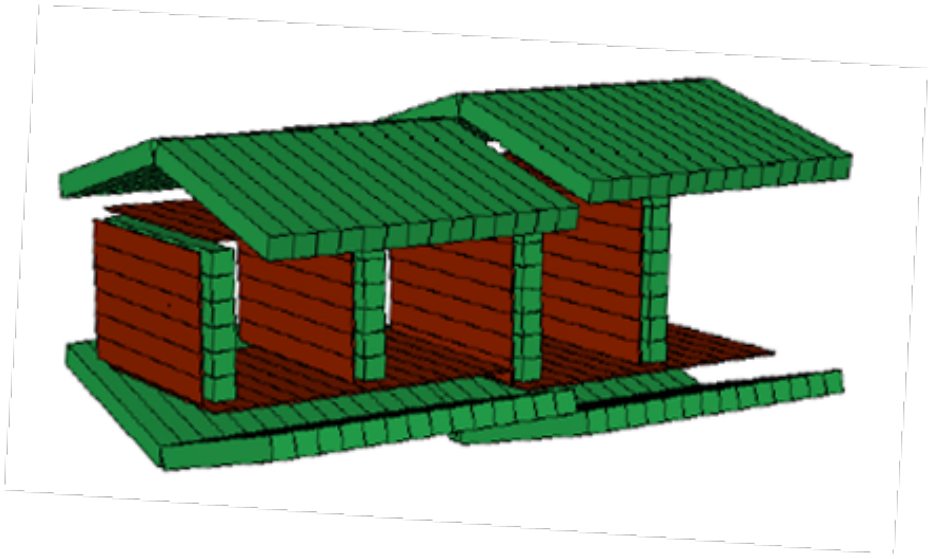

Figure 2.2 Neutron polarimeter design

From the up down asymmetries, ξ, of the neutrons, a better concept of the charge distribution inside of the neutron can be conceptualized. Results from this experiment can provide improved tests against concurrent lattice QCD models. In this experiments as well as in all physics experiments in Hall-C SHMS will play a major role in achieving the required detection of charged particles, their energy, tracking and particle ID.

CHAPTER 3

Quartz Hodoscope

3.1 Super High Momentum Spectrometer

The quartz hodoscope will be a part of the detector package that goes in the SHMS. The spectrometer SHMS consists of magnets in combination with detector package in the detector hut. The spectrometer uses a QQQD configuration where the three quadrupoles are used as focusing elements to bring the particles to the detector hut[5]. The dipole then bends and focuses the scattered particles towards the focal plane inside the detector package. The refocused particles are then detected by a series of scintillators or in the case of the SHMS, scintillators and the quartz hodoscope, to trigger a Cherenkov Counter for particle ID, a lead glass calorimeter for energy movement, and wire chambers for tracking purposes.

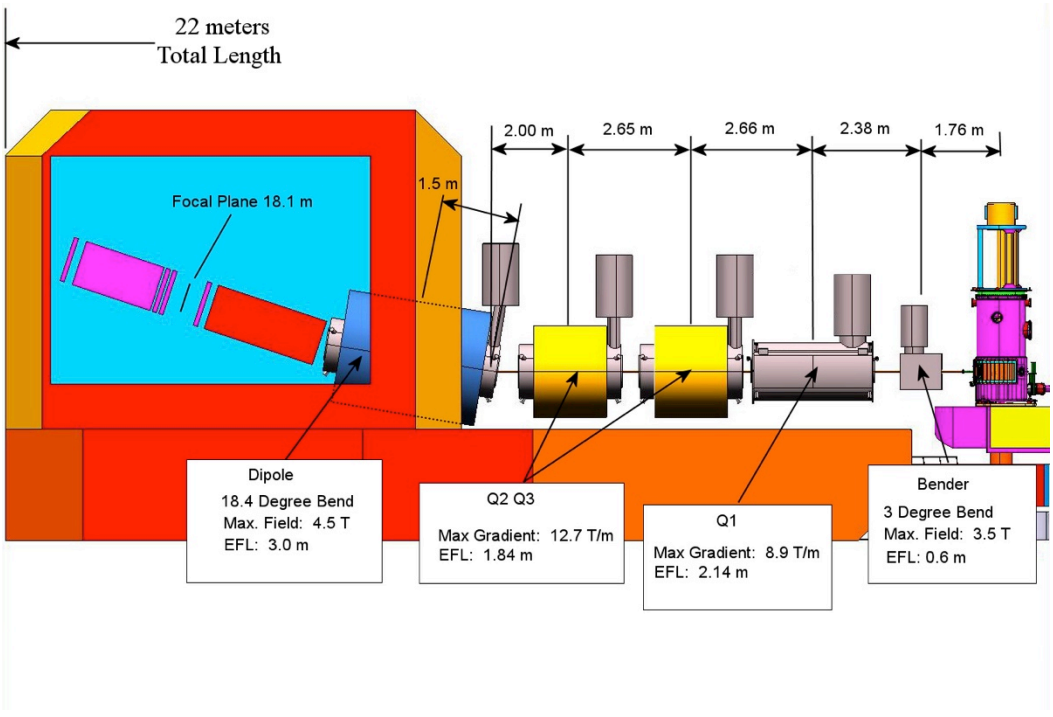

Figure 3.1. Diagram of the SHMS

The SHMS detector package allows for particle identification, event timing, momentum determination, and particle trajectory tracking[6].

3.2 Design

The quartz hodoscope was developed to be a part of the Super High Momentum Spectrometer. This hodoscope is the fourth in a line of 3 scintillator planes in the SHMS detector. Figure 3.1 shows a rendering of the SHMS detector hut with the quartz hodoscope.

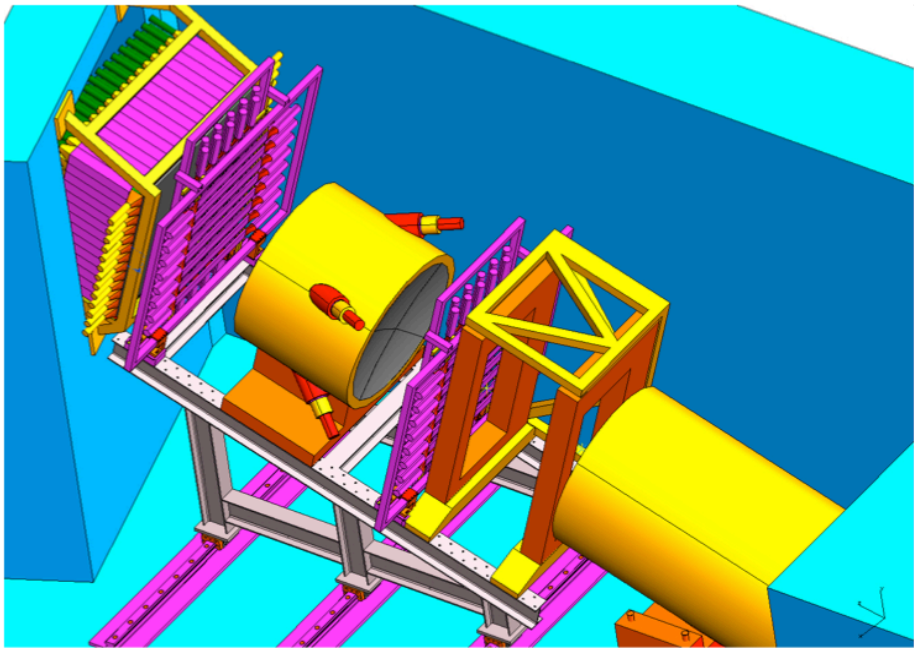

Figure 3.2 Detector hat

The hodoscope was designed to detect particles that scattered in the experimental target. That scattered particles form a 120 by 120 cm beam envelope at the location of the hodoscope[4]. The picture shown in figure 3.2 shows the distribution of particles in the beam envelope with the majority of particles found towards the center of the package with less particles towards the outside of the envelope.

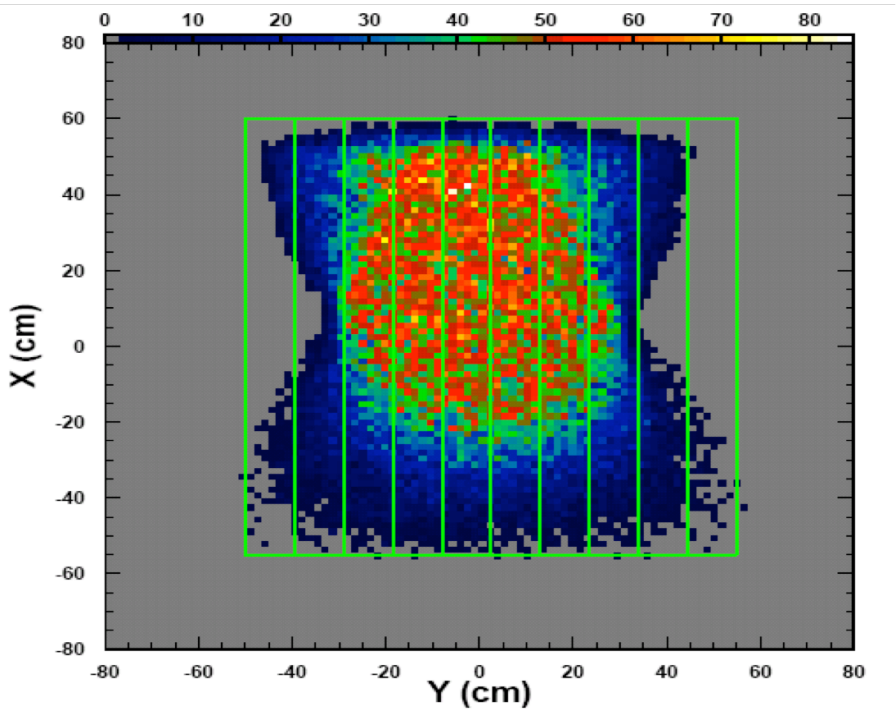

Figure 3.3 Beam envelope

Once installed in the SHMS, the quartz hodoscope will provide a clean detection of charged particles, a high level of background rejection, and accurate tracking efficiency determination.

3.3 Hodoscope Physics Background

What allows the quartz hodoscope to distinguish the high-energy particles from the background noise is the combination of two physics concepts: the Cherenkov effect and the total internal reflection process.

3.3.1 The Cherenkov Effect. The Cherenkov effect occurs in a medium when a particle exceeds the speed of light for a medium while inside aforementioned medium. This phenomenon causes an electromagnetic wave front of cone like shape to be formed following the particle. The angle of the cone depends on the speed of the particle, $\beta = v/c$, and a refractive index, n, as defined by the following formula:

$$\cos\theta = \frac{1}{n\beta}$$

Because the Cherenkov radiation relies on a threshold velocity, to display the effect, all particles below this threshold of $\beta = 1/n$ where n is the index of refraction of the medium at a given wavelength[7]. Specifically the index of refraction of the quartz bars within the quartz hodoscope is around 1.46. This leads to a threshold, β, of around 0.68 and a Cherenkov angle of approximately 43.4° for fast particles ($\beta > 0.9$).

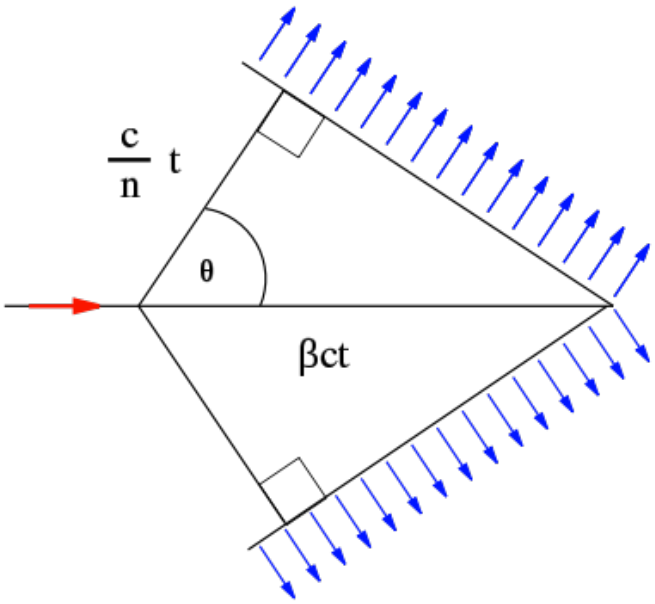

Figure 3.4 Cherenkov effect diagram

3.3.2 Total internal reflection. When a particle is incident on one of the quartz bars in the hodoscope and that particle has a high energy it can exhibit the Cherenkov effect. This effect can be combined with the effect of total internal reflection. Total internal reflection dictates that when a propagating light impacts a medium boundary at an angle larger than the critical angle, the light remains inside the medium and is completely reflected. Combining this phenomenon with the Cherenkov effect allows for a high-energy particle incident on a quartz bar

perpendicular to the surface, to propagate an light wave of a 200-400 nm wavelength throughout the entire bar until reaching the photomultiplier tubes on either end of the bar.

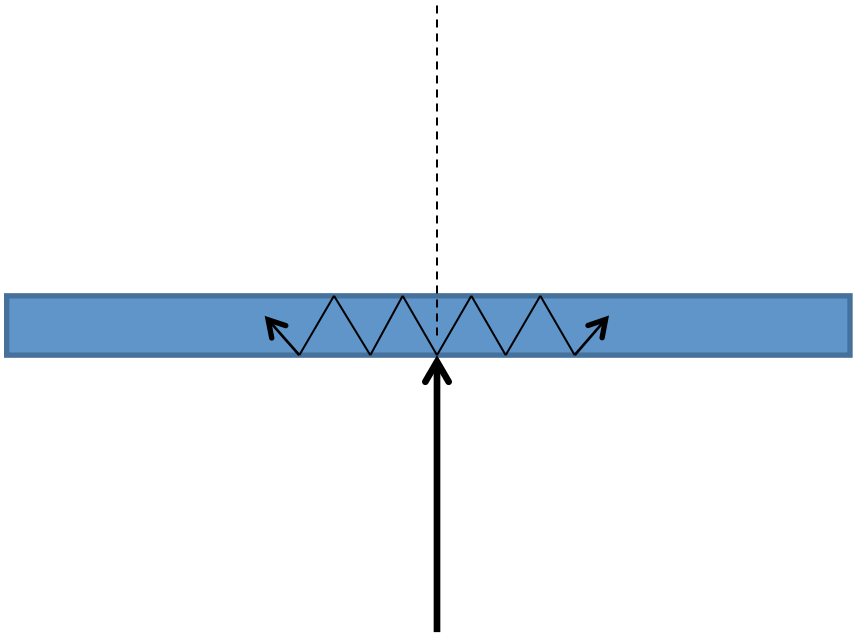

Figure 3.5 Total internal reflection simulation

These two developments together can push the β threshold to around .92 essentially filtering a large percentage of the low energy background noise due to randomly impact particles detected by the PMT's. This process allows the quartz hodoscope to suppress background noise and trigger the SHMS when the energy level of particles are detected and not by background events.

3.3.3 Ultraviolet Sensitive PMT's. The PMT's on the ends of the quartz bars were specially designed and selected to be highly sensitive to light on the lower wavelength of the light spectrum. This is important, as the hodoscope needs to detect as many high-energy photons as for the trigger system to maintain high efficiency.

CHAPTER 4

Hodoscope Construction & Calibration

The quartz hodoscope was designed as a combination of 21 quartz bars measuring 125 by 5.5 by 2.5 cm^3 and 42 UV spectrum sensitive photomultiplier tubes.

4.1 Wrapping and Taping

Construction began by cleaning the quartz bars of any and all dust and debris using alcohol and chemical wipes. This is to ensure that there are no trapped dust particles that can affect the transmission of the produced Cherenkov light that propagates by total internal reflection throughout the bar.

Figure 4.1 Unwrapped quartz bar

Each of the quartz bars was fully wrapped twice by a sheet of around 47μm thick tedlar paper with a thin pocket of air between the bar and the paper to ensure total internal reflection. Next a line of black scotch tape was placed down each side of the bar to secure the tedlar. The bars were wrapped tightly that no debris could fit between the paper and the bar.

Figure 4.2 Wrapped quartz bar

4.2 Brace Assembly and Application

Next the braces that would be the interface between the quartz bars and the PMTs were assembled. The braces consisted of combining four anchoring pieces connected to a steel bar interface and a Styrofoam buffer. These pieces were bound with an adjustable circular steel clamp.

Figure 4.3 PMT brace components

4.3 PMT-Quartz Bar bonding

A silicon compound gel, RTV615A, was used to bond the PMT to the quartz bar within the metal brace. This compound was chosen because of its index of refraction, $n \approx 1.41$, which was close to the index of refraction of the quartz bars, $n \approx 1.406$.

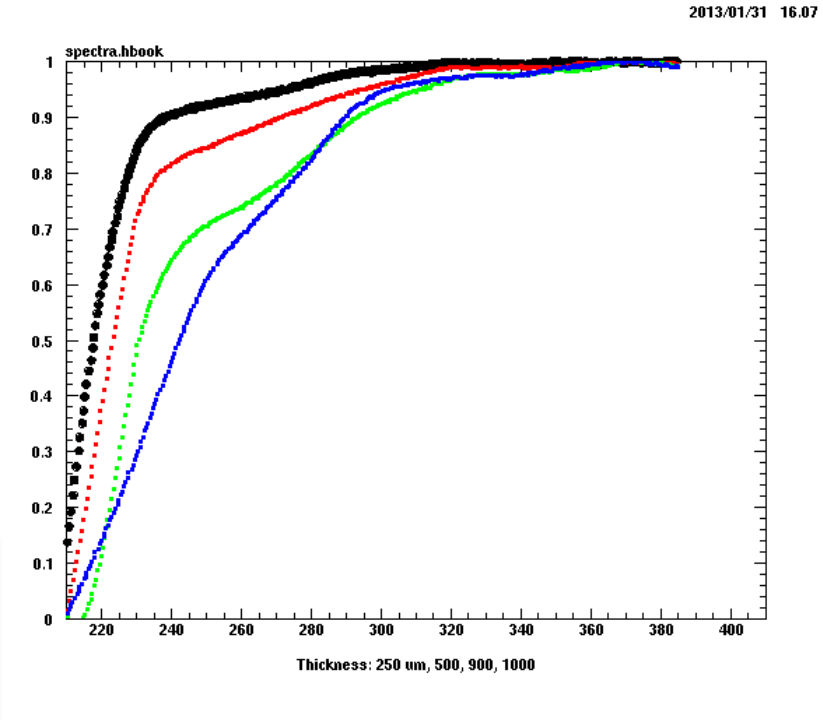

Figure 4.4 Transmission vs. thickness

The silicon compound was composed of a mixture of a silicon compound and a curing agent. These two parts were then mixed with a 10-part silicon, 1 part curing agent ratio.

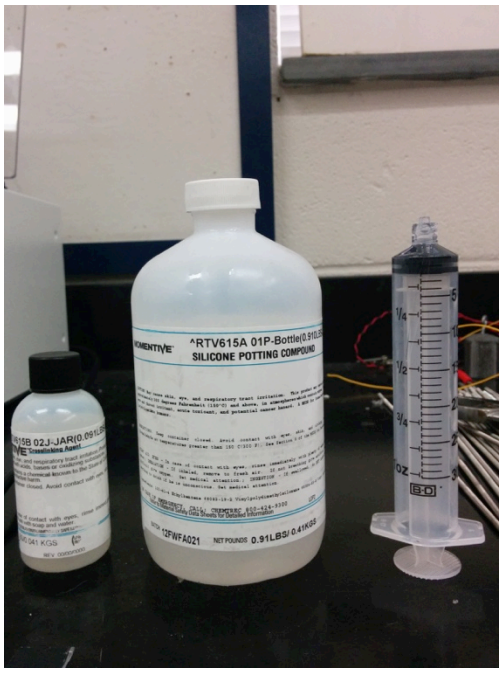

Figure 4.5 Silicon compound components

The mixture was run through a centrifuge for fifteen minutes before being applied to the lens of previously cleaned PMT's. It was determined that the thickness of the compound needed to be around 9mm in order to completely cover the PMT lens while providing adequate light transmission. After removing any air bubbles, the compound was allowed to settle and completely spread. Next the PMT's were placed upon the quartz bar-braces and gently tightened from the back for security. They were allowed to cure for 8-10 hours before the bars were flipped to the upside down to apply PMT's to the opposite sides. Each completed bar was placed in a large wooden transport brace that kept it secure for storage and transport.

Figure 4.6 Quartz bar storage rack

4.4 PMT Calibration

All PMT's were tested in the black box. Some of them were calibrated on the subject of single photoelectron peak at different high voltage values. For this calibration, a PMT would be placed inside of a large dark box, *Figure 4.7*, where they would be isolated from other light sources.

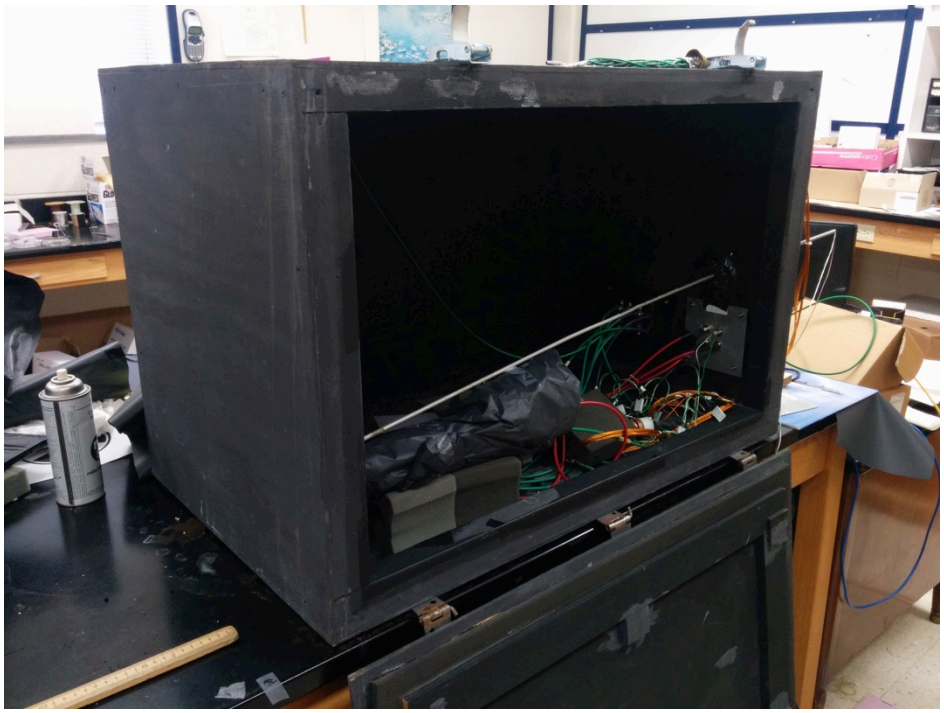

Figure 4.7 Light isolated box

Inside this box, a single LED was placed close to the PMT's photocathode. The LED was connected to a signal generator where the pulse, frequency, and intensity could be monitored and adjusted delicately. By monitoring a digital oscilloscope, it could be determined how much of light the PMT was receiving. The LED position and generator settings were adjusted accordingly until the strongest signal became apparent on the oscilloscope. Then the signal from the PMT was sent to an ADC or amplitude to digital converter, which was then recorded through the Data Acquisition System (DAQ) on the computer. After analyzing the amplitude graphs, the optimal high voltage values were chosen. Then the PMT's were cleaned so that they could be glued to the quartz bars.

4.5. Hodoscope Calibration

Once five of the bars had completed construction, they were situated horizontally and connected to power sources and computers as seen in *Figure 4.8*.

Figure 4.8 Rack of quartz bars

This process of calibration entailed attaching two scintillating paddles, on top and bottom of the rack to determine the timing of the bars. Cosmic muons would come impact the top paddle and pass through each of the bars on their way to the bottom paddle. The trigger would signal when four out of the five bars and the paddles in coincidence detected the particle and recoded an event. The position of the scintillators were set at one end of the rack, then moved ~10 cm along the bar each time until the opposite end of the rack was reached. The signals from the PMT's

were sent to the electronics setup, to set the timing window as well as detect the amplitude of each recorded event. The electronics diagram for the measurement is shown in *figure 4.9.*

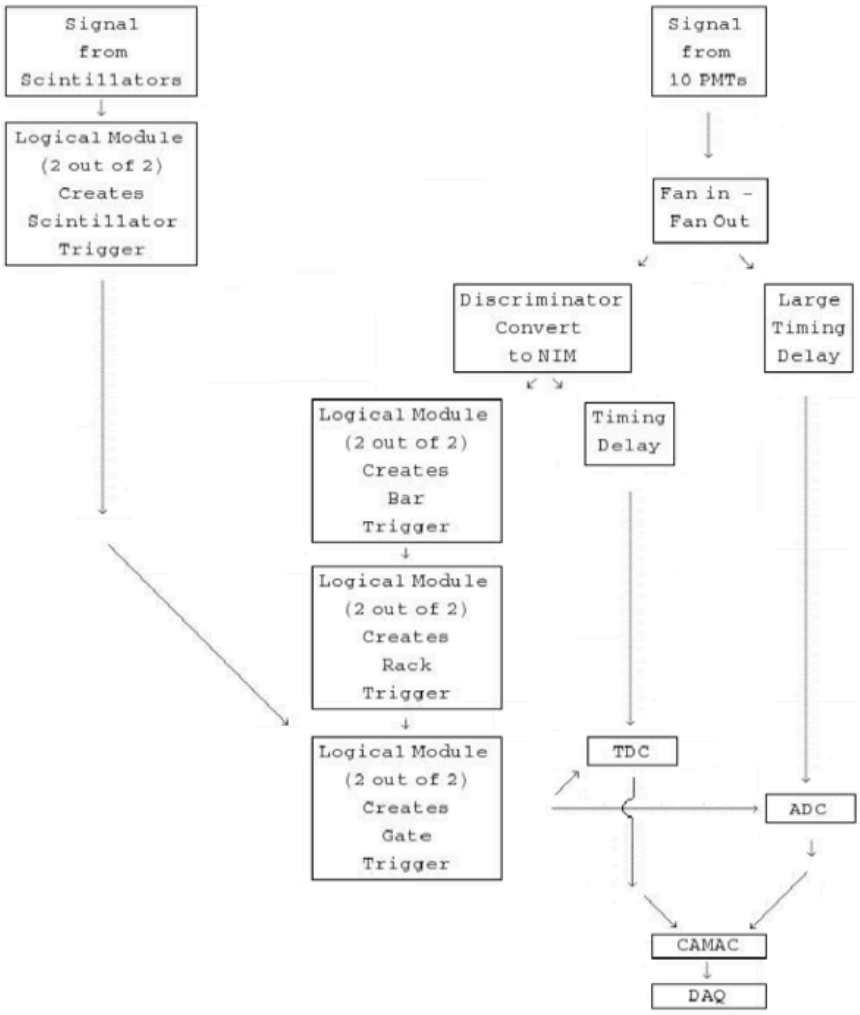

Figure 4.9 Electronics data path

CHAPTER 5

Data Analysis

5.1 Histogramming & Fitting

Using a program known as the Physics Analysis Workstation or PAW++, a program was compiled to take the inputs of the raw ADC and TDC values and compile them into histograms. Some of graphs were fitted with an applicable function for determining the amount of photoelectrons detected by the hodoscope while others were used to determine the timing resolution at each scintillator paddle position for each bar.

5.2 Timing Resolution Data

The timing histograms in *Figure 5.1* are a graphical interpretation of how long it takes for an event to reach each of the two PMT's on the sides of the quartz bars.

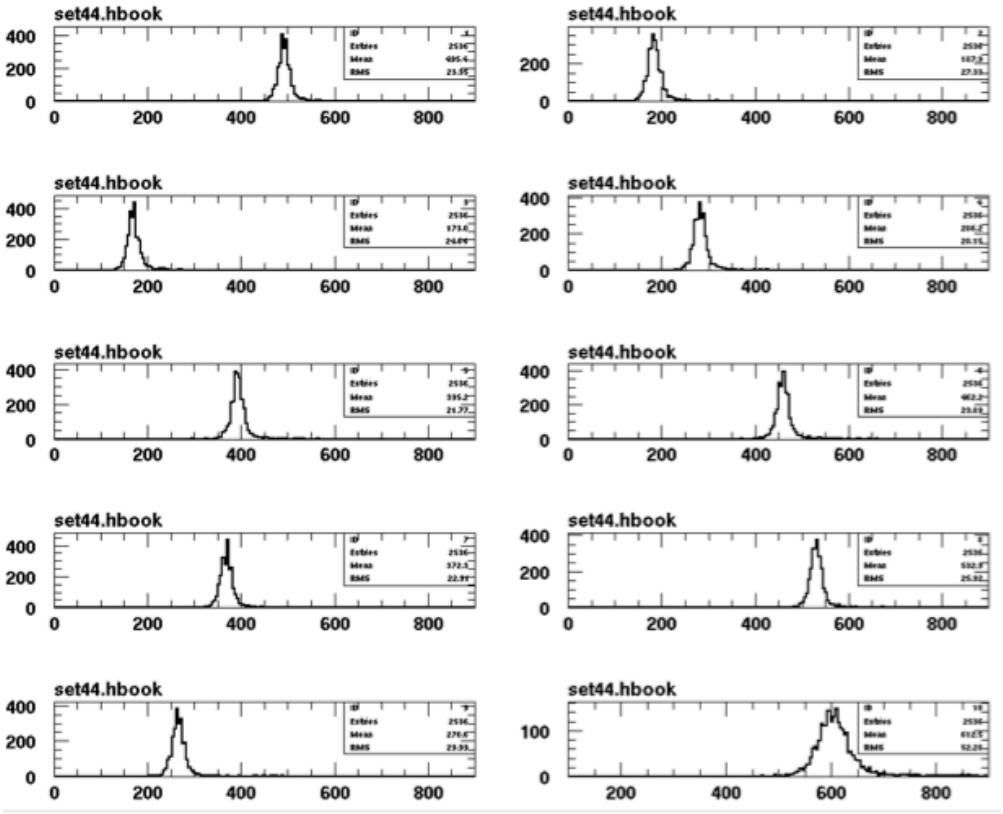

Figure 5.1 Sample of raw timing histograms from data set 44

The timing histograms from *Figure 5.1* and others are then compiled into a cumulative histogram for each position. These aggregate graphs show the amount of events recorded at each position relative to how long they take to reach the surrounding PMT's.

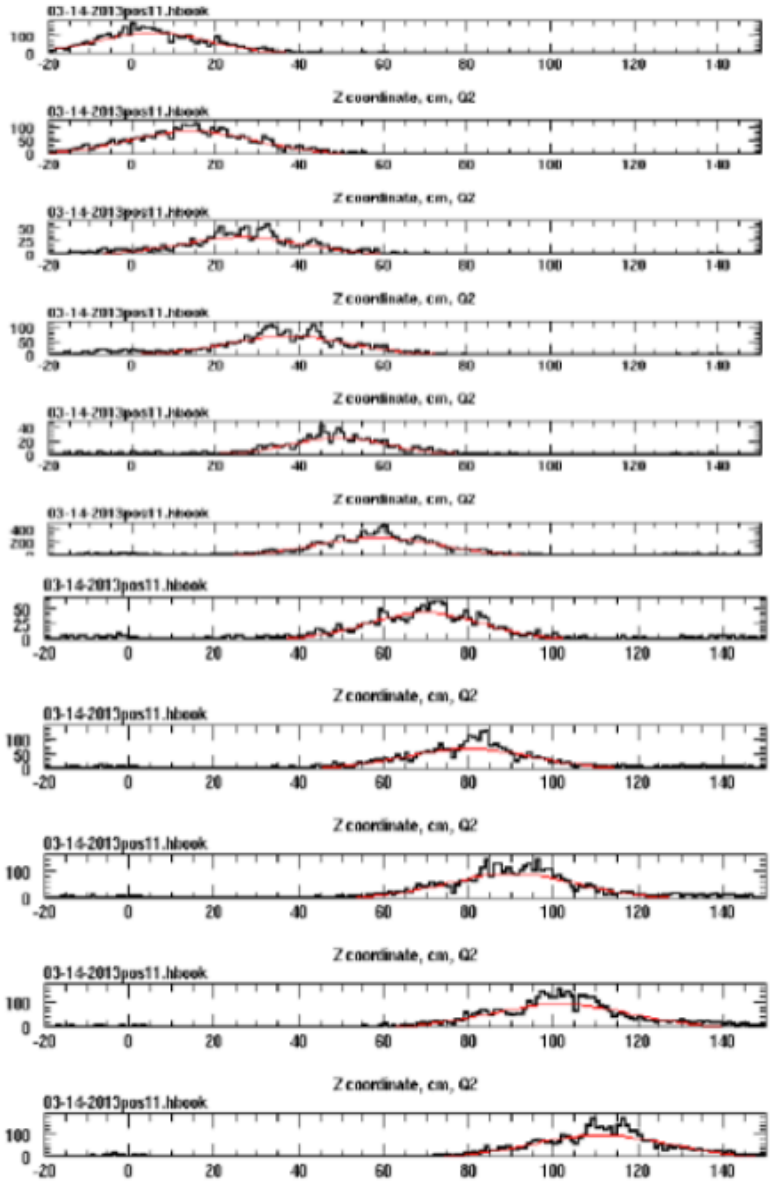

Figure 5.2 Aggregate Timing

These readings show a correlation between the positioning of the scintillating paddles and the timing of the signals from each PMT.

Figure 5.3 shows a direct comparison of the position measured versus the set position of the paddle.

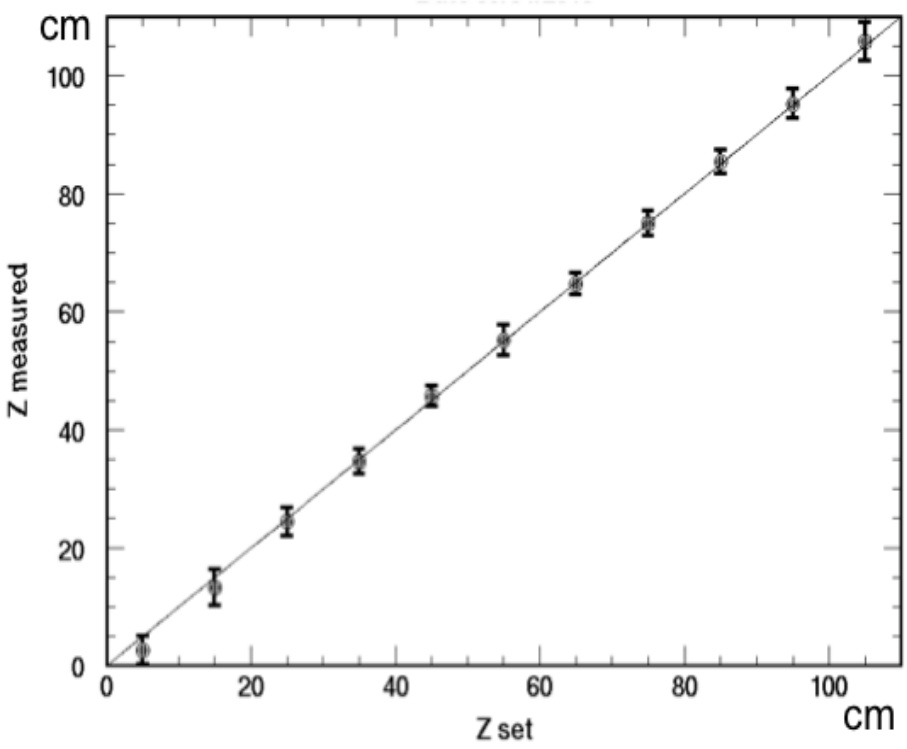

Figure 5.3 Position Reconstruction

5.3 Amplitude Data

Measuring the amplitude of the signal meant taking the ADC data from the PMT's for each event, and checking the raw amount of events recorded over a period of time. These amplitude graphs were entered into PAW++ and then fitted with fits to give measurement parameters. After the graphs are compiled, they can be used to count the amount of photoelectrons that the PMT's detected per time period. The histograms were fit with Gaussian and Poisson distributions depending on the natural shape of the graph. *Figure 5.4* gives examples of amplitudes data from data sets before they are fitted with functions.

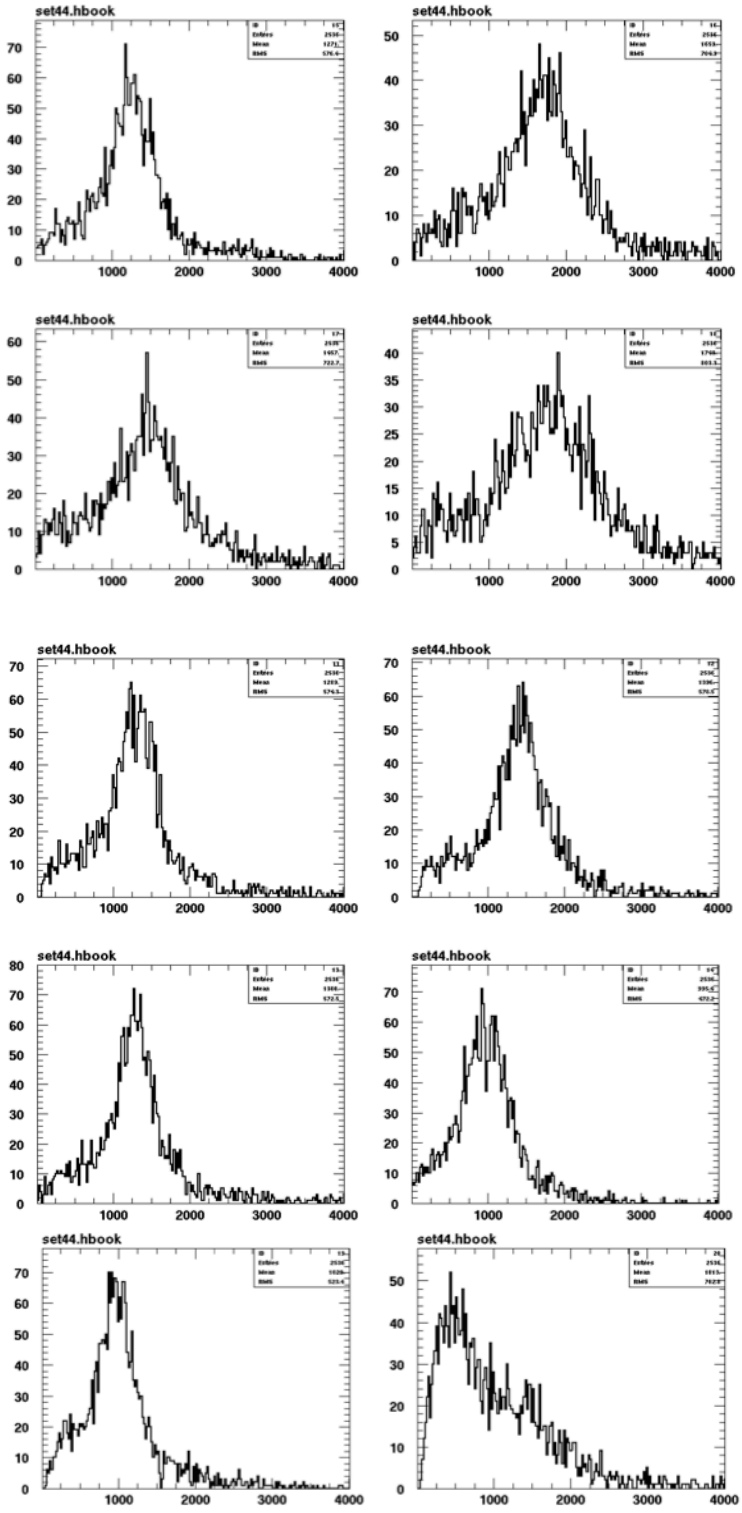

Figure 5.4 Sample of raw amplitude histograms from data set 44

5.4 Photoelectron Calculation

Two of the main options for calculating the photoelectrons off an amplitude histogram involve fitting either a Gaussian or a Poisson trend to the data. Both of these fits output parameters that can essential in calculating the number of photoelectrons.

5.4.1 Gaussian fit. The Gaussian fit on a graph, gives a relatively easy method of calculating the number of photoelectrons by using the peak and standard deviation statistics. Using *Figure 5.5* as an example, one can see that a Gaussian function adjusts perfectly around a bell curve.

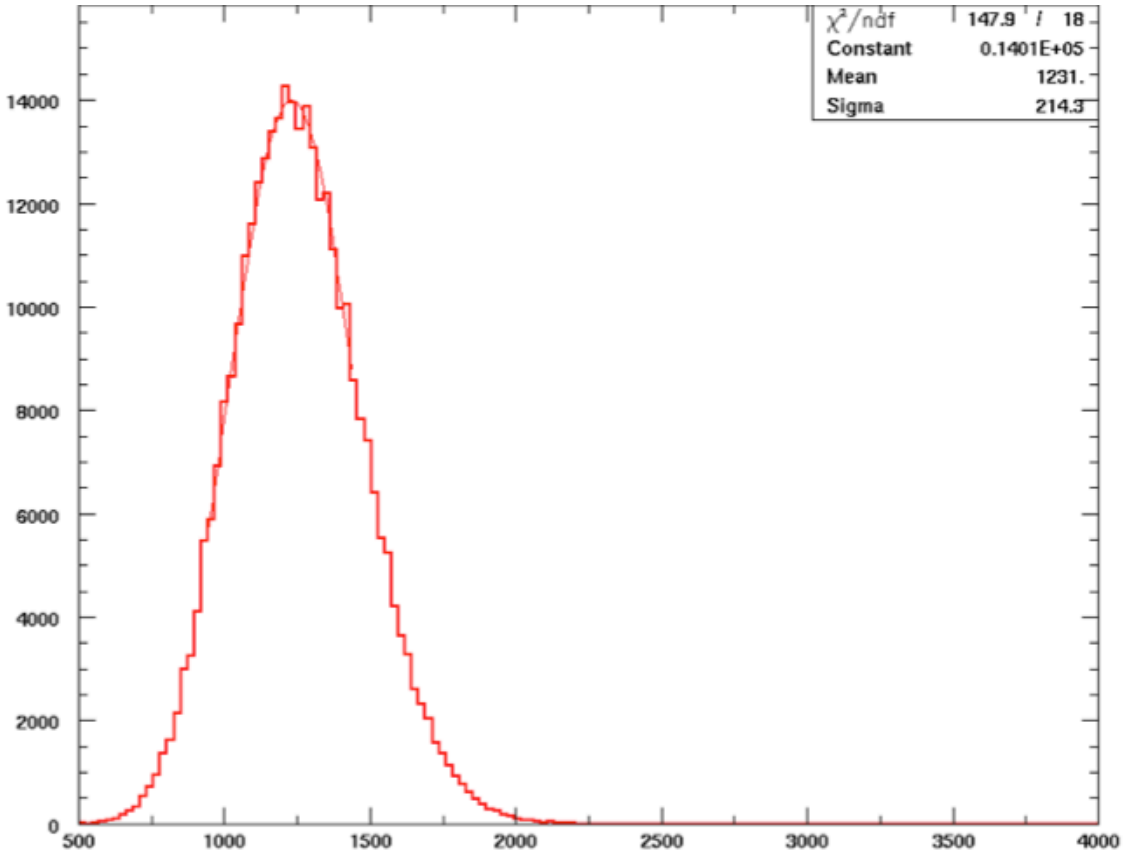

Figure 5.5 Gaussian Fit on an ADC histogram

The number of photoelectrons from this fit can be calculated by taking the square of the mean, μ_0, over the standard deviation, σ_{0m} as shown by *Figure 5.6*[8].

$$n_0 = (\frac{\mu_0}{\sigma_{0m}})^2$$

Figure 5.6 Photoelectron calculation equation

The amount of photoelectrons for this specific graph with a mean of 1231 and a sigma of 214.3 is given by *Figure 5.7*

$$n_{p.e.} = (\frac{1231}{214.3})^2 \approx 33$$

Figure 5.7 Sample photoelectron calculation

5.4.2 Poisson fit. The Poisson fit is more applicable where there is more than a few photoelectrons detected. Fitting this function to a curve outputs several parameters, including Q_1, *which* is the number of ADC channels for a PMT. Taking this value in conjunction with the peak from a bell curve gives another photoelectron calculation.

The Poisson fit is more applicable when performing the calibration on PMT's where it's more likely to see the single photoelectron peak. This method shows the amount of light it takes for a PMT to see a single photoelectron.

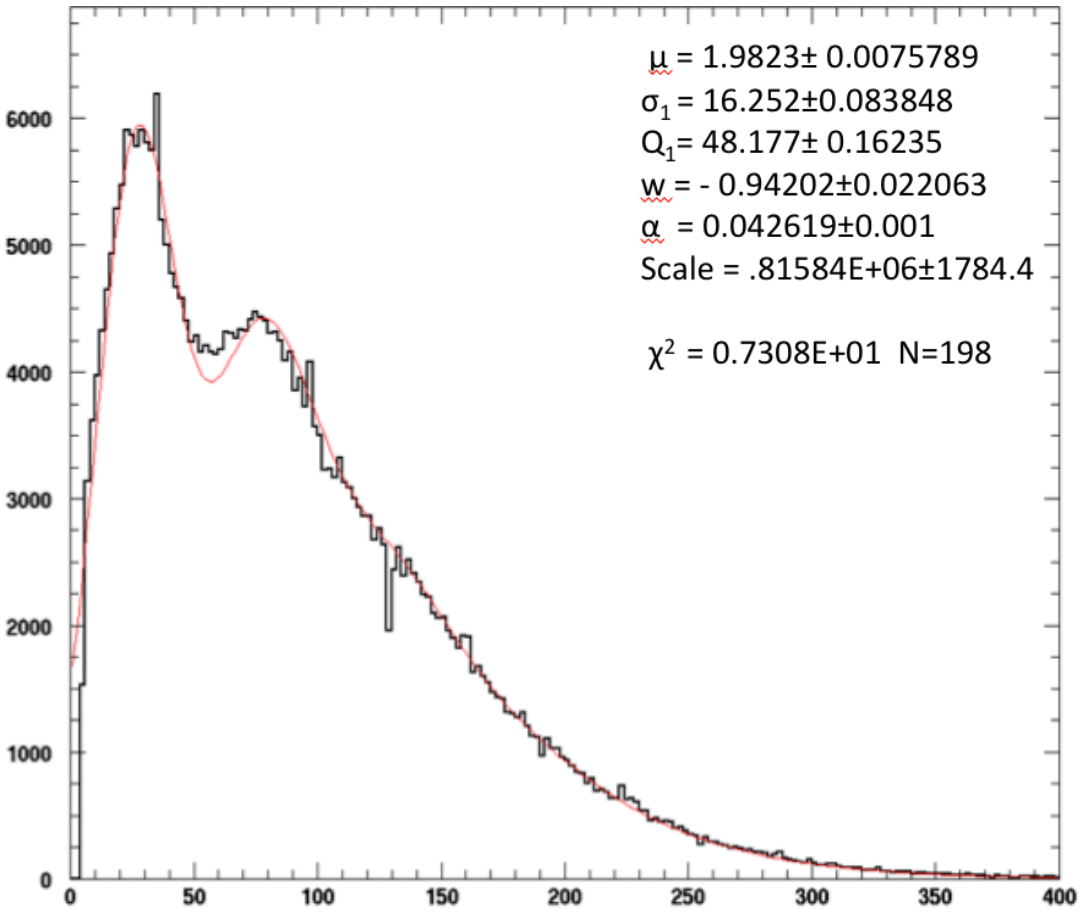

Figure 5.8 The Poisson curve fitted to a single electron peak graph

The Poisson fit on this histogram gives a Q_1 of 48.177. Taking this parameter and the mean value from *Figure 5.5* one can estimate the number of photoelectrons potentially given from this PMT with the given number of ADC channels.

$$n_{p.e.} = (\frac{1241}{48.177}) \approx 26$$

Figure 5.9 Photoelectron calculate for a Poisson fit

CHAPTER 6

Results and Conclusion

A quartz hodoscope has been constructed at North Carolina A&T. This quartz hodoscope has been designed to function in the SHMS detector at Jefferson Lab in Hall-C. It has been extensively calibrated and tested for the sensitivity to UV light and detection of high number of photoelectrons.

Results indicate that at least 25 photoelectrons are detected per PMT. Position resolution was also established to be within 1.5 and 2.0 cm of the hodoscope center. Future work is still needed to demonstrate efficiency.

References

1. About Jefferson Lab | Jefferson Lab. Retrieved August 29, 2014 from http://www.jlab.org/about-jefferson-lab

2. 12 GeV Upgrade: Future at Jefferson Lab – Unique Opportunities. Retrieved August 10, 2014, from http://www.jlab.org/12GeV/unique.html

3. Huber, G.M., Lolos, G.J., Papandreou, Z. Measurement of the Charged Pion Form Factor High Q^2, 2006, Retrieved October 20, 2014 from http://www.jlab.org/exp_prog/proposals/06/PR12-06-101.pdf

4. Bosted, P., Brooks. W., Bruell, A., Dharmawardane, V., Ent, R., Gaskell, D., Horn, T., Jones, M.K., Measurement of the Ratio $R = \sigma_L/\sigma_T$ in Semi-Inclusive Deep-Inelastic Scattering, 2006, Retrieved October 20, 2014 from http://www.jlab.org/exp_prog/proposals/06/PR12-06-104.pdf

5. Arrington, J., Geesaman, D.F., Hafidi, K., Holt, R., Potterveld, D.H., Riemer, P.E., Solvignon, P., Inclusive Scattering from Nuclei at $X > 1$ in the quasielastic and deeply inelastic regimes, 2006, Retrieved October 20, 2014 from http://www.jlab.org/exp_prog/proposals/06/PR12-06-105.pdf

6. Zhou, S., Li, X., A Path to "Color Polarizabilities" in the Neutron: A Precision Measurement of the Neutron g_2 and d_2 at High Q^2 in Hall C

7. Horn, T, SHMS – Experiments, 2009. Retrieved August 12, 2014, from http://www.jlab.org/Hall-C/upgrade/12gev_experiments.html

8. Anderson, B.D, The Neutron Electric Form Factor at Q^2 up to 7 $(GeV/c)^2$ from the Reaction^2 $H(e,e,n)^1H$ via Recoil Polarimetry, 2012, Retrieved October 20, 2014 from http://www.jlab.org/exp_prog/proposals/11/PR12-11-009.pdf

9. Horn, T., SHMS – detector locations and beam envelope, 2008. Retrieved October 25, 2009 from https://www.jlab.org/Hall-C/upgrade/HALLC_12GEV/shms_beam_envelope.html

10. Villano, Anthony N., Neutral pion electroproduction in the Delta resonance region, 2007, Retrieved October 16, 2014 from http://books.google.com/books?isbn=0549455167

11. Mack, D.J., A Scintillating Hodoscope for the SHMS, 2002. Retrieved August 11, 2014, from https://www.jlab.org/Hall-C/talks/04_09_02/Mack2.pdf

12. Cerenkov Effect. Retrieved August 28, 2014 from https://teachers.web.cern.ch/teachers/archiv/HST2002/Bubblech/mbitu/cerenkov_effect.htm

13. Adamson, P., Photoelectron Counting by Several Methods, 2000. Retrieved June 9, 2014 from http://minos-docdb.fnal.gov/0006/000661/001/numi0661.ps.gz